ACTA ASTRONOMICA
Vol. **67** (2017) pp. 0–0

Variable Stars in M13. II. The Red Variables and the Globular Cluster Period–Luminosity Relation

W. Osborn[1], A. Layden[2], G. Kopacki[3], H. Smith[4], M. Anderson[4], A. Kelly[2], K. McBride[2] and B. Pritzl[5]

[1] Yerkes Observatory, 373 West Geneva Street, Williams Bay, WI 53191, USA
Dept. of Physics, Central Michigan Univ., Mount Pleasant, MI 48859, USA
e-mail:Wayne.Osborn@cmich.edu
[2] Dept. of Physics & Astronomy, Bowling Green State Univ., Bowling Green, OH 43043, USA
e-mail: laydena@bgsu.edu
[3] Instytut Astronomiczny, Uniwersytet Wrocławski, ul. Kopernika 11, 51-622 Wrocław, Poland
e-mail: kopacki@astro.uni.wroc.pl
[4] Dept. of Physics & Astronomy, Michigan State Univ., East Lansing, MI 48824, USA
e-mail: smith@pa.msu.edu
[5] Physics & Astronomy Dept., Univ. of Wisconsin Oshkosh, Oshkosh WI 54901, USA
e-mail: pritzlb@uwosh.edu

Received March 21, 2017

ABSTRACT

New CCD observations have been combined with archival data to investigate the nature of the red variables in the globular cluster M13. Mean magnitudes, colors and variation ranges on the $UBVI_C$ system have been determined for the seventeen cataloged red variables. Fifteen of the stars are irregular or semi-regular variables that lie at the top of the red giant branch in the color–magnitude diagram. Two stars are not, including one with a well-defined period and a light curve shape indicating it is an ellipsoidal or eclipsing variable. All stars redder than $(V-I_C)_0 = 1.38$ mag vary, with the amplitudes being larger with increased stellar luminosity and with bluer filter passband. Searches of the data for periodicities yielded typical variability cycle times ranging from 30 d up to 92 d for the most luminous star. Several stars have evidence of multiple periods. The stars' period–luminosity diagram compared to those from microlensing survey data shows that most M13 red variables are overtone pulsators. Comparison with the diagrams for other globular clusters shows a correlation between red variable luminosity and cluster metallicity.

Key words: *globular clusters: individual (M13) – stars: individual (M13 red variables)*

1. Introduction

This is the second paper in a series focusing on the variable stars in the globular cluster M13 (NGC 6205 = Cl 1639+365). Paper I (Osborn 2000) gave positions and average $UBVR_CI_C$ photometry for most of the variable stars then known as well as for stars suitable as local comparison stars for the cluster's RR Lyr and Cepheid variables. Soon after a paper by Kopacki, Kołaczkowski and Pigulski (2003, hereafter KKP03) appeared that contained a comprehensive re-discussion of the work on the M13 variables to that time and presented V and I_C observations, in flux units, from an image subtraction analysis of new CCD observations. This Paper II of the series now presents a detailed discussion of the bright red variables of M13 making use of both the KKP03 results and those from the new observations. Future papers will treat the cluster's Cepheid and RR Lyr variable stars.

That some of the brightest and reddest members of globular clusters are variable has been known at least since the early observations of ω Cen by Bailey (1902). Nevertheless, these variables have been little studied in comparison to the clusters' RR Lyr and Cepheid variables and until recently relatively little was known about the nature of their variations. This lack of attention can be attributed mainly to the fact that observations with exposure times and time coverage designed to investigate the short-period variables, as are most common, are poorly suited for also studying the brighter red variables whose variation timescales require observations over months

The brightest globular cluster red variables are asymptotic giant branch (AGB) stars while the fainter ones – those below the brightness level of the tip of the red giant branch – are a mixture of AGB and red giant branch (RGB) stars. In both cases the stars have extended atmospheric envelopes and their variability likely results from a combination of pulsation and convection (Catelan and Smith 2015). Frogel and Elias (1988) showed that the AGB stars are undergoing mass loss, and the effect of stellar instability on the mass loss rate affects a star's evolution. More recently, Lebzelter and Wood (2005) have shown that mass loss must occur on the RGB as well in order for stellar pulsation models to match the observed period–luminosity (PL) relations. Untangling the relative importance of pulsation, convection and mass loss to model the brightness variations requires better and longer observational coverage than has typically been available.

An outcome from gravitational microlensing surveys (*e.g.*, MACHO, OGLE, EROS) has been a very large amount of observational data on variable stars in several fields, especially the Magellanic Clouds and the Galactic bulge (Cook *et al*. 1995, Kiss and Bedding 2004a, Soszyński *et al*. 2009, Kim *et al*. 2014 and references therein). These data have significantly increased understanding of red variables, but have also demonstrated the complex and heterogeneous nature of such objects. As examples, the microlensing observations reveal at least seven sequences in the PL diagram corresponding to different stellar populations and pulsational modes, that stars may pulsate in several modes simultaneously (or even

switch modes) and that there are possible period changes resulting from thermal pulses (see, for example, Wood *et al*. 1999, Kiss and Lah 2006, Takayama, Saio and Ita 2013, Soszyński, Wood and Udalski 2013 and references therein). Schultheis, Glass and Cioni (2004) and Soszyński *et al*. (2007) detected a dependence of pulsational properties on metallicity. Nevertheless, to date the metallicity domain for the variability for these stars has been poorly explored, especially as regards very metal-poor stars. Observational data for globular cluster red variables, whose metallicities are well known, provide a path toward clarifying the situation.

The past fifteen years have seen progress on obtaining the observational data needed to understand globular cluster red variables. CCD-based studies by Lebzelter and Wood (2005, 2011, 2016) on 47 Tuc, NGC 362, NGC 2808, and ω Cen and by Abbas *et al*. (2015) on NGC 6496, have resulted in the discovery of many low-amplitude red variables, as well as variables in the cluster cores where crowding had complicated earlier photographic studies. A significant fraction of these variables show light curves with a "long secondary period" of unknown origin (see Percy *et al*. 2004, Wood *et al*. 2004, Nichols *et al*. 2009) superimposed on their more-rapid pulsational light variations.

CCD monitoring of the M13 red variables began in 2001 with the observations reported by KKP03. Soon after, a team of observers led by F.A. Violat Bordonau – hereafter the Violat Team – began posting a series of reports on the bright variables in M13 on

http://casanchi.com

a Spanish-language "publication site" for mathematics, physics and astronomy[1]. Their small telescopes, having 20–35 cm aperture and located at various locations in Spain, enjoy long periods of clear weather which allowed the brighter M13 variables to be followed from 2001 through 2013 with the data for each observing season typically covering 4–6 months with good cadence. The resulting *V*-band light curves, and sometimes radial velocities from the literature, were used to confirm the variability of suspected variables, determine amplitudes and mean magnitudes and search for periods. Their findings for specific stars are discussed in the Appendix in comparison with those from this study.

This paper presents the results of a new study of the M13 red variables undertaken with two main goals. First, we wanted to use well-calibrated photometry to determine the basic light curve parameters of the stars in the $UBVI_C$ system: mean magnitudes, colors and amplitudes. Second, we wanted to investigate the nature of the variations: general forms of the light curves, typical cycle durations, cycle to cycle and long-term changes, periodicities present. Attaining these goals requires

[1] As examples, see
http://casanchi.com/ast/v1101.pdf,
http://casanchi.com/ast/rojas.pdf,
http://casanchi.com/ast/rojas02.pdf, hereafter VA07b,
http://casanchi.com/ast/m13a01.pdf, hereafter VB15.
The full list of the Team's papers on M13 red variables can be found in the on-line Appendix.

quality photometry spanning months to years with a cadence of days to weeks. We present such photometry in Section 2. The results from these observations combined with all other available photometry are given in Section 3 with the details on a star-by-star basis in the Appendix.

2. The Observational Material

While most red giants show variability at some level, we define the M13 red variables as only those stars so listed in the online "Catalogue of Variable Stars in Galactic Globular Clusters" (Clement 2013)[2] and shown to have detectable variations by KKP03 or, for the stars they did not study, by other investigators. Seventeen stars met these criteria. These are listed in Table 1 along with their corresponding Ludendorff (1905) numbers, mean brightness $\langle V \rangle$, and reported range of brightness ΔV (C13, Sandquist *et al*. 2010).

T a b l e 1

Red variables of M13

Variable	Lud.	$\langle V \rangle$ [mag]	ΔV [mag]	Variable	Lud.	$\langle V \rangle$ [mag]	ΔV [mag]
V11	324	11.93	0.13	V38	414	12.12	0.07
V15	835	12.14	0.09	V39	629	11.98	0.22
V17	973	11.98	0.38	V40	940	12.08	0.08
V18	72	12.32	0.11	V41	782	13.16	0.11
V19	194	12.07	0.09	V42	289	11.94	0.10
V20	70	12.12		V43	96	12.47	0.07
V24	598	12.01	0.24	V44	445	12.12	
V32	66	14.10	0.24	V45	554	12.59	
V33	954	12.09					

2.1. CCD Data

New CCD photometry of the M13 red variables has been obtained using telescopes at the Michigan State University (MSU), Macalester College (Macal.), Bowling Green State University (BGSU) and Wrocław University Białków Station observatories. Data were obtained in the period 2003–2014. In addition, the 2001 observations of KKP03 at Białków have been re-reduced to obtain magnitudes. Table 2 summarizes the telescope apertures, the filters employed, and the observing seasons. We have data for all seventeen confirmed red variables in M13. Our CCD photometry of the red variables is available in the online Appendix.

MSU and Macalester Observations

The MSU data were obtained with a 0.6-m Cassegrain reflector equipped with an Apogee Ap47p CCD camera for observing seasons 2003–2005 and with an

[2] *http://www.astro.utoronto.ca/~cclement/read.html*, hereafter C13

T a b l e 2

New CCD data of M13

Observatory	Telesc.	Filters	Observing seasons
Białków	0.6-m	V, I_C	2001
MSU	0.6-m	B, V	2003, 2004, 2006, 2008, 2009, 2010
Macalester	0.4-m	B, V	2004
BGSU	0.5-m	V, I_C	2006, 2007, 2009, 2010, 2011
Białków	0.6-m	B, V, I_C	2014

Apogee Alta U47 Camera for the 2006–2010 seasons. These cameras had a $10' \times 10'$ field of view and scales of 1.2 arcsec/pixel and 0.6 arcsec/pixel, respectively. The Macalester observations were obtained in 2004 with a 0.4 m reflector and an SBIG ST-8 CCD camera which produced a $13' \times 8'$ field of view and 0.5 arcsec/pixel scale. Seeing was typically $3''$–$4''$, and occasionally worse, at both locations.

Images were obtained in B, V and I_C with both telescopes and were processed in an identical manner. They were bias, dark and flat field corrected and instrumental magnitudes then determined using the DAOPHOT profile-fitting reduction package (Stetson 1987, 1994). Because the observations were originally designed to study the short-period Cepheid variables, many of the I_C-band images of the bright red variables have saturation problems and the I_C data have not been used. Some V images also approached saturation and were excluded from consideration.

The instrumental b and v magnitudes were reduced to the standard system using equations of the form:

$$V = v + a_1(b-v) + c_1 \qquad B = b + a_2(b-v) + c_2. \tag{1}$$

The color terms were determined from observations of Landolt standards and stars within the open cluster M67 (Landolt 1992, Schild 1983, 1985). When good observations could not be made through both filters, the color at the time of observation was estimated from the star's typical color. Eight to ten uncrowded local standard stars were used to transform each frame, using standard B and V values from Osborn (2000) and Stetson (2000). The very red colors of the variables complicated the selection of standard stars, but standards as red as $B-V = 1.5$ mag were included.

BGSU Observations

The BGSU observations were acquired with a 0.5-m Cassegrain telescope and Apogee Ap6e CCD camera in the observing seasons listed in Table 2. The field of view was $21' \times 21'$ with $1\farcs2$ pixels and the median seeing was $3\farcs1$. Images were taken in V and I_C, with the cluster visited once each night, each visit consisting of four images per filter dithered to prevent stars from repeatedly landing on bad

pixels. The raw images were processed in the standard way and then the images from each night were combined to produce one, clean, high signal-to-noise image in V and one in I_C for that night.

Instrumental magnitudes were next obtained, for most stars using the DAOPHOT PSF-fitting software following the method described in Abbas *et al*. (2015), and transformed to the standard system using equations analogous to Eq.(1). For variables in the cluster core, the Alard and Lupton (1998) image subtraction method (ISM) was applied to the central subregion of the CCD field and magnitudes then obtained using coefficients derived from uncrowded stars common to both the DAOPHOT and ISM data sets.

Białków Observations

The 2001 Białków observations are from the earlier work of KKP03 where the observing equipment and reduction procedures are described. These observations have been re-reduced to have magnitudes rather than fluxes as in the original work. The 2014 observations were made using an Andor DW432-BV back-illuminated CCD camera (see Kopacki *et al*. 2008 for a more detailed description). The seeing ranged from $1\farcs7$ to $4\farcs0$ with $2\farcs4$ being typical. Both sets of data were reduced using the ISM technique and the DAOPHOT package. Those ISM light curves of stars lying outside the cluster core were converted to instrumental magnitudes using their DAOPHOT light curves, which in turn were transformed to standard system using Stetson's (2000) data.

2.2. Other Observations

We have also accumulated and used as many sets of individual observations of the red variables as we could locate. Some of these had been published (Demers 1971, Pike and Meston 1977, Russev 1973, Russev and Russeva 1979a, 1979c, Russeva, Illiev and Russev 1982), but in a number of cases we secured from papers' authors observations used in their studies but not published. These latter include observations by Russev and collaborators (Russev and Russeva 1979b, Russeva and Russev 1980, Russev private communication), Welty (1985) and Osborn (2000, adopting Osborn-L to refer to that paper's photoelectric observations made at Lowell Observatory and Osborn-N to refer to the photographic ones made at the U.S. Naval Observatory – Flagstaff Station). We received some preliminary data from the Violat Team, but these have been neglected in favor of their results published online. This additional observational material is heterogeneous, containing photoelectric $UBVR_CI_C$ measures, photographic UBV data and unfiltered photographic magnitudes. The earliest observations are from 1962. The previously unpublished observations are given in the Appendix.

2.3. Summary of the Available Data

Section 4 of the Appendix gives tables listing, for each red variable, the number of nights of observations (and in parentheses the total number of observations) in

each observing season for the different passbands. Observations are available from the 1962 through the 2014 seasons in B, with coverage 1976–2014 in V and 1991–2014 in I_C. This collection of observations allows us to study the variations over an unprecedented time period.

2.4. Consistency between Data Sets and Adopted Mean Magnitudes

We have looked at the various data sets to see if there are any significant systematic differences between those of the same passband. We do not have many contemporaneous measures and the stars vary. Therefore our comparison generally is based on average magnitudes for the data sets, but recognizing that sets with little time coverage may be unreliable because observations spanning only a portion of a pulsation cycle may not produce a reliable average brightness.

Table 3 shows how the average V from the different observation sets compare. The first nine lines show the mean magnitudes for those data sets listed in Sections 2.1–2.2 for which we have the individual measures. The type of photometry is indicated (CCD, pe = photoelectric photometry, pg = photographic photometry) with the CCD data sets listed first. Values from sets with limited time coverage are in italics. The next lines show published magnitudes from independent photometry for which we do not have the individual measures. These are from the CCD observations of Guarnieri, Bragaglia and Fusi Pecci (1993, hereafter GBF), Rey *et al*. (2001), Sandquist *et al*. (2010), Stetson (2000)[3] and the Violat Team[4] followed by the older photoelectric and photographic photometry of Arp and Johnson (1955), Cathey (1974) and Kadla (1966). Finally, there is photometry from HST images by Cohen *et al*. (1997, hereafter CGY) for the two most difficult stars to study – V44 and V45 in the very core of the cluster. The bottom row of Table 3 has our adopted mean V for each star. These are weighted averages with the CCD and long-time coverage data given higher weight and ignoring obviously discordant values, which are in smaller type and enclosed in parentheses in the table. The final column of Table 3 lists the average difference between the measures for that data set and our adopted values. One sees that with a few exceptions the sets agree well.

Table 4 presents the data for the I_C observations in the same form as for the V data. There are fewer data sets, but again the agreement between them is excellent. However, a review of the individual data points indicated that most of the Białków images in 2001 of V19, V38, V40, and V42 were saturated.

The U comparisons are presented in Table 5. The data are quite limited and show more scatter than for the other passbands. The only CCD data is from Stetson (2000). Surprisingly, a comparison of Stetson's U values with those from Arp and Johnson (1955) for the twenty M13 stars in common revealed a systematic difference of 0.10 mag for all but the most blue ($B-V < 0.0$ mag) stars. This

[3]Available at *http://www.cadc-ccda.hia-iha.nrc-cnrc.gc.ca/en/community/STETSON/standards/*; the latest version no longer lists data for V20 and V33.

[4]The listed values are the averages of those published in the various papers listed in the Appendix.

same difference was found between Stetson's results and other M13 photoelectric data. Stetson's U values are based on Landolt (1983, 1992) standards, and a number of authors have pointed out there are differences between the Landolt and Johnson systems, particularly in $U-B$ (*e.g.*, Bessell 1990, Menzies *et al*. 1991).

The mean-magnitude comparisons for B are given in Table 6. There are seven sets of CCD photometry, but only two have data for more than half the stars and both of these cover only limited time spans. There are fairly extensive photographic data.

Tables 3–6 reveal several problems with the photometric data besides that with U. The GBF B and V magnitudes are systematically bright by about 0.20 mag, as was previously reported by Osborn (2000)[5]. The Sandquist *et al*. (2010) photometry for V17 is overly faint. Rey *et al*. (2001) values are systematically 0.10 mag bright for his two brightest stars (V18 and V20). The Violat Team noted that their measures of V42 are compromised by its close companion. The Demers (1971) observations are too bright in V and B (and probably in U). These anomalous data have been ignored in the determinations of the adopted mean magnitudes. Magnitude measures for the four variables in the crowded regions of the cluster (V24, V39, V44, V45) are difficult and are less consistent than for the other stars. Failure to properly correct for background stars, or close companions as in the case of V42, can lead to erroneous magnitudes, and there is the suggestion that this is the case for the BGSU and the Violat Team observations of those five stars. The adopted values for these variables are therefore more uncertain than for the others. For the remaining twelve stars we adopt errors for our mean values of 0.01 mag for V and $I_{\rm C}$, 0.02 mag for B and 0.06 mag for U.

For V and $I_{\rm C}$, all CCD data (other than the problem cases mentioned) agree within a few hundredths of a magnitude. The differences between our most extensive data sets – the Białków and BGSU CCD measures in V and $I_{\rm C}$ – average 0.005 mag and -0.009 mag respectively for the fifteen stars in common. The agreement between our results and the independent photometry indicates there are no significant zero-point errors. This result includes the more uncertain photographic data and the Violat Team CCD observations, some of which were unfiltered. We conclude that V and $I_{\rm C}$ data from the different sources can be combined in our analyses.

For B the agreement between the CCD and photoelectric data is good, but the photographic observation sets have average offsets up to 0.09 mag relative to the CCD photometry. The scatter among the various U measures combined with the unexplained systematic difference discovered between Stetson's CCD U results and those from photoelectric observations indicate the U data sets have zero-point uncertainties of about 0.10 mag. In spite of these issues, for our analyses we have elected to combine the B and U data from the different data sets without making any adjustments.

[5]The $B-V$ values are consistent with other measures.

Table 3

Comparison of the average V from different data sets

Ref	Type	V11	V15	V17	V18	V19	V20	V24	V32	V33	V38	V39	V40	V41	V42	V43	V44	V45	Dif.
Białków	CCD	11.90	12.10	11.99	12.32	12.04	*12.06*	11.99	*14.13*	*12.03*	12.11	11.97	12.08	13.15	11.91	12.44			−0.01
BGSU	CCD	11.92	12.12	12.02	12.33	12.10	12.09	11.93	14.11	12.06	12.09	11.83	12.06	13.09	11.93	12.46	12.03	12.46	−0.01
MSU	CCD	12.02	12.10	11.97		12.08					12.12		12.07	13.09					0.00
Macal.	CCD	12.02	12.12	12.07		12.06					12.19		12.05	13.12					0.03
Osb.-L	pe		(12.21)	12.00	12.32		12.10			12.11	12.16								0.04
Osb.-N	pg	11.91	12.15	11.95	12.30	12.06	11.99	12.01		12.06	12.12	11.99	12.07						−0.01
Welty	pg	*11.98*	*12.17*	*11.96*	*12.43*	*12.05*	*12.05*		*14.15*	*12.01*	*12.16*			*13.20*		*12.44*			0.02
Pike-M.	pg	11.94					12.15												0.05
Demers	pg	(11.76)																	−0.17
CGY	CCD																*12.14*	*12.65*	0.04
GBF	CCD		(11.87)								(11.88)	(11.76)							−0.22
Rey	CCD				(12.20)		(11.97)		14.11							12.49			0.02
Sandq.	CCD		12.13	(12.29)	12.31	12.08	12.12	11.96	14.14	12.01	12.07	11.98	12.09	13.22	11.99	12.45	12.12	12.59	0.01
Stetson	CCD				12.31	12.08			14.13		12.12					12.44			0.00
Viol. T.	CCD	12.03	12.14	12.02	12.33	12.14	12.10	(12.13)		12.13	12.11	(12.14)	12.06	13.23	(11.78)	12.44			0.04
Arp-Jo.	pe						12.03												−0.05
Cathey	pe				12.32		12.12		14.10	12.09						12.52			0.03
Kadla	pg		12.09	12.04	12.34	12.23	12.18		14.12	12.11	12.14			13.14		12.51			0.03
ADOPT		11.91	12.12	12.00	12.32	12.08	12.08	11.97	14.12	12.05	12.11	11.96	12.07	13.14	11.94	12.44	12.11	12.59	

Table 4

Comparison of the average I_C from different data sets

Ref	Type	V11	V15	V17	V18	V19	V20	V24	V32	V33	V38	V39	V40	V41	V42	V43	V44	V45	Dif.
Białków	CCD	10.36	10.67	10.46	10.96	10.58	*10.53*	10.39	*13.28*	*10.53*	10.65	10.45	10.65	11.98	10.45	11.14			0.00
BGSU	CCD	10.37	10.67	10.49	10.97	10.60	10.55	10.35	13.27	10.53	10.63	10.34	10.64	11.93	10.47	11.14	10.62	11.30	−0.01
Osb.-L	pe				*10.98*		*10.49*			*10.53*									−0.01
CGY	CCD																*10.81*	*11.59*	0.12
Sandq.	CCD		10.68	(10.62)	10.95	10.56	10.56	10.37	13.34	10.50	10.62	10.42	10.66	12.05	10.50	11.15	10.71	11.41	0.01
Stetson	CCD				10.96	10.60			13.30		10.66					11.15			0.01
ADOPT		10.36	10.67	10.47	10.96	10.59	10.53	10.37	13.29	10.52	10.64	10.42	10.65	11.97	10.46	11.14	10.72	11.44	

Table 5

Comparison of the average U from different data sets

Ref	Type	V11	V15	V17	V18	V19	V20	V24	V32	V33	V38	V39	V40	V41	V42	V43	V44	V45	Dif.
Osb.-L	pe		*15.04*	15.05	14.82		15.35			15.27	15.03								−0.03
Osb.-N	pg	*15.16*	*15.14*	*15.21*	*15.04*	*15.27*	*15.38*	*15.27*		*15.32*	*15.26*	(*15.6*)	*15.09*						0.11
Demers	pg	14.94																	−0.11
Stetson	CCD				14.69	15.13			14.79		15.00					14.67			−0.03
Arp-Jo.	pe						15.42												0.02
Cathey	pe				14.78		15.40		14.91	15.27						14.88			0.00
Kadla	pg				14.78		15.42												0.01
ADOPT		15.05	15.07	15.10	14.79	15.16	15.40	15.27	14.87	15.30	15.05	15.6	15.09			14.76			

Table 6

Comparison of the average *B* from different data sets

Ref	Type	V11	V15	V17	V18	V19	V20	V24	V32	V33	V38	V39	V40	V41	V42	V43	V44	V45	Dif.
Białków	CCD	*13.46*	*13.52*	*13.63*	*13.66*	*13.52*	*13.57*	*13.61*	*14.81*	*13.53*	*13.60*	*13.53*	*13.59*	*14.28*	*13.37*	*13.67*			−0.01
MSU	CCD	13.44	13.62	13.53		13.49					13.58		13.57	14.21					−0.02
Macal.	CCD	13.43	13.67	13.60		13.45					13.57		13.57	14.26					−0.00
Osb.-L	pe		*13.59*	13.50	13.61		13.65			13.64	13.57								−0.01
Osb.-N	pg	13.50	13.62	13.50	13.61	13.57	13.58	13.61		13.61	13.58	13.58	13.55						0.00
Welty	pg	13.58	13.66	13.60	13.67	13.65			14.82	13.63	13.58			14.40		13.75			0.06
Russev	pg	13.40	13.58	13.56	13.68	13.71	13.70	13.77	14.81										0.05
Pike	pg	13.53					13.76												0.09
Demers	pg	(13.39)																	−0.07
GBF	CCD		(13.46)								(13.30)	(13.43)							−0.18
Rey	CCD				(13.51)		(13.53)		14.78							13.79			0.03
Sandq.	CCD		13.61	(14.08)	13.58	13.51	13.64	13.60	14.77	13.58	13.57	13.61	13.56	14.31	13.48	13.65	13.55	13.70	−0.01
Stetson	CCD				13.62	13.58			14.79		13.57					13.70			−0.00
Arp-Jo.	pe						13.61												−0.04
Cathey	pe				13.62		13.71		14.73	13.63						13.79			0.02
Kadla	pg		13.56	13.62	13.56	13.83	13.66		14.75	13.60	13.61			14.25		13.77			0.00
ADOPT		13.46	13.59	13.56	13.62	13.57	13.65	13.61	14.78	13.59	13.58	13.56	13.57	14.26	13.41	13.72	13.55	13.70	

3. Results and Analysis

3.1. Mean Magnitudes and Colors

We have B, V and I_C magnitudes for all seventeen red variables, but only limited data for V44 and V45. We have uncertain U data for twelve of the stars. Our adopted mean magnitudes in Tables 3–6 yield $\langle V \rangle$ and M_V (the mean and absolute V magnitudes) and colors of the stars given in the initial columns of Table 7. M_V has been computed using $(V - M_V) = 14.33$ mag and $E(B-V) = 0.02$ mag (Harris 2010).

T a b l e 7

Mean V, M_V , colors and variation amplitudes for the M13 red variables

Star	$\langle V \rangle$ [mag]	M_V [mag]	$U-B$ [mag]	$B-V$ [mag]	$V-I$ [mag]	ΔB [mag]	ΔV [mag]	ΔI [mag]
V11	11.91	−2.42	1.59	1.55	1.55	0.50	0.30	0.17
V15	12.12	−2.21	1.48	1.47	1.45	0.26	0.10	0.06
V17	12.00	−2.33	1.54	1.56	1.53	0.37	0.35	0.21
V18	12.32	−2.01	1.17	1.30	1.36	0.27	0.10	0.08
V19	12.08	−2.25	1.59	1.49	1.49	0.40	0.17	0.08
V20	12.08	−2.25	1.75	1.57	1.55	0.30	0.16	0.09
V24	11.97	−2.36	1.66	1.64	1.60	0.30	0.22	0.13
V32	14.12	−0.21	0.09	0.66	0.83	0.30	0.08	0.07
V33	12.05	−2.28	1.71	1.54	1.53	0.26	0.15	0.07
V38	12.11	−2.22	1.47	1.47	1.47	0.23	0.13	0.07
V39	11.96	−2.37		1.60	1.54	0.26	0.25	0.18
V40	12.07	−2.26	1.52	1.50	1.42	0.26	0.14	0.09
V41	13.14	−1.19		1.12	1.17	0.45	0.17	0.12
V42	11.94	−2.29		1.47	1.48		0.17	0.14
V43	12.44	−1.89	1.04	1.28	1.30	0.21	0.09	0.05
V44	12.11	−2.22		1.44	1.39		0.12	0.09
V45	12.59	−1.74		1.11	1.15		0.11	0.06

3.2. Variables in the Color–Magnitude Diagram

Fig. 1 shows the positions of the M13 variables in the cluster's color–magnitude diagram. The crosses showing the color–magnitude diagram branches are from those stars in Stetson's (2000) list of M13 photometric standards that are located within 5′.0 of the cluster center and, when known, are astrometric cluster members (Cudworth and Monet 1979, Cudworth 1979). The symbols for stars independently confirmed not to vary (Osborn 2000, KKP03, Violat Team[6]) are circled. We have

[6] *http://casanchi.com/ast/fijas.pdf, http://casanchi.com/ast/M13_200401.pdf, http://casanchi.com/ast/l93801.pdf*

used $E(V-I_C) = 1.35\,E(B-V)$ (Bergbusch and Stetson 2009) to obtain the unreddened colors. The red variables are plotted as circles (those with uncertain data not filled in) and the locations of the three Cepheids (V1, V2 and V6) and the RR Lyr variables are also indicated. The positions of V41 and V32 show these are not typical red variables. All stars redder than $(V-I_C)_0 = 1.38$ mag are confirmed variables. This color, which corresponds to $M_V = -2.25$ mag, indicates where variability becomes significant as stars brighten due to evolution.

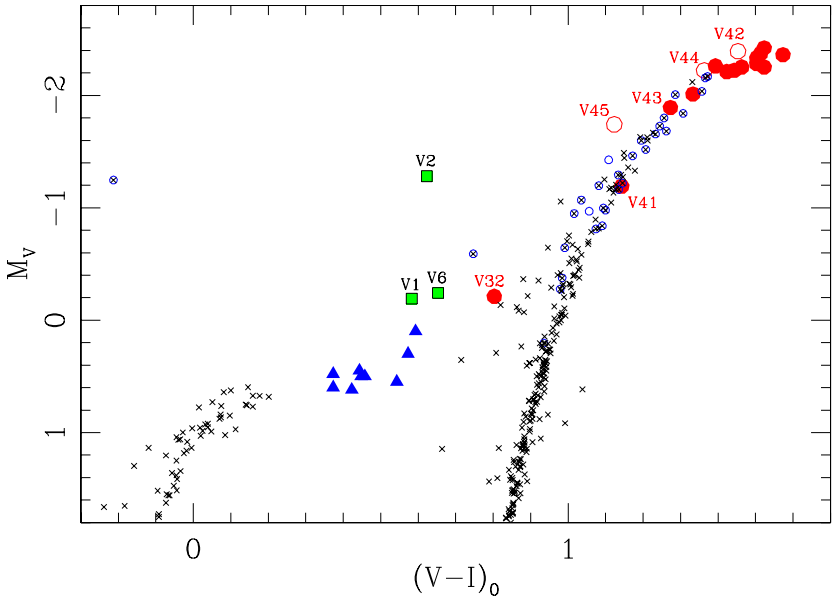

Fig. 1. Color–magnitude diagram of M13 showing the variable stars. Red variables are plotted as circles (those with uncertain data not filled in), Cepheids as squares and RR Lyr stars as triangles. Confirmed non-variables are circled crosses.

3.3. Variation Amplitudes

V11 is the star with the most extensive data which cover the period 1962–2014. Fig. 2 shows its MSU and BGSU B, V and I_C light curves for two observing seasons. The fact that the observations from different telescopes and for different passbands show similar rises and falls in brightness demonstrates that the observed variations are real and not some artifact of our photometric measures. Fig. 3 shows the light curve for V11 compared to that for V15 from all available V data and plotted with the same magnitude scale. The V11 magnitudes have larger spread than those of V15, and the dispersion of observed magnitudes provides an indicator of the typical range of variation.

We used a combination of the standard deviation about the mean and the observed full range for all observations in a given passband as our measure of variation amplitude. For most stars the B observations included photographic data extending to earlier decades compared with the V-band date range shown in Fig. 3, while for

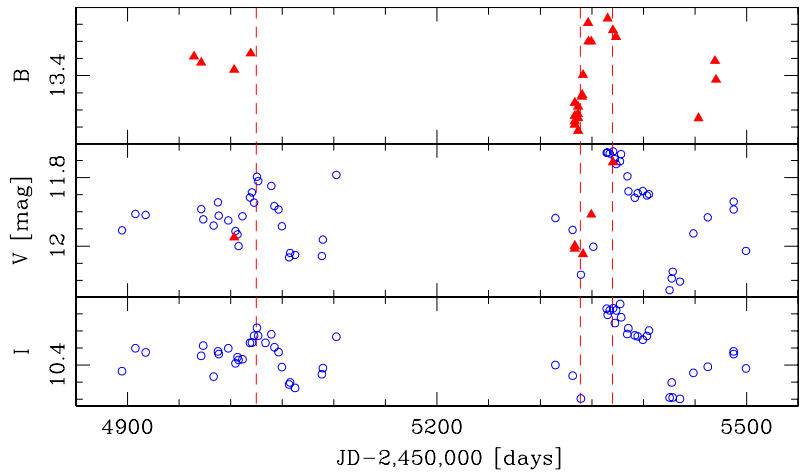

Fig. 2. Our time-series CCD data for V11 in BVI_C for the two observing seasons 2009 and 2010. Filled triangles indicate data from MSU and open circles are from BGSU. The dates of two maxima and one minimum are indicated with vertical lines. The changes in brightness agree for both the different passbands and for the observations taken with different telescopes. The magnitude scale tick marks show 0.05 mag intervals.

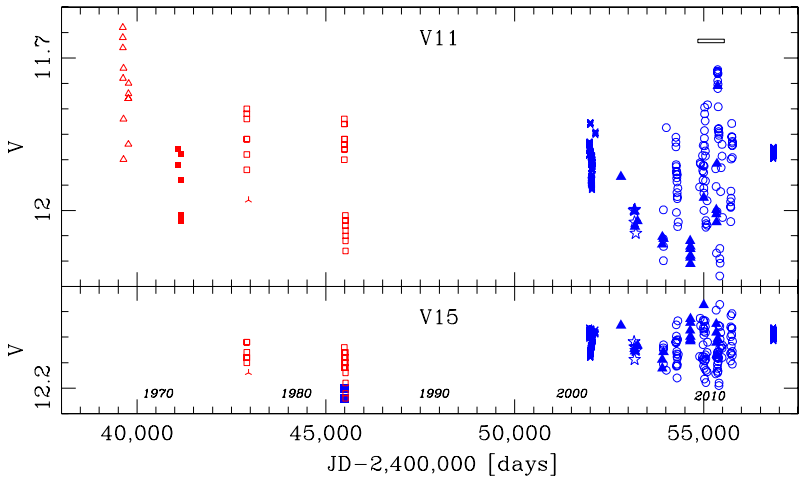

Fig. 3. Photographic and CCD time-series *V*-band data for V11 (*top*) and V15 (*bottom*) showing the difference in variation amplitude. Symbols indicate data from the following sources (from *right* to *left*): open triangles – Demers (1971), solid squares – Pike and Meston (1977), 3-point cross – Welty, open squares – Osborn-N, filled squares, Osborn-L, dense 4-point crosses – Białków, filled triangles – MSU, open stars – Macalester, open circles – BGSU. Data from before 1990 (red) are photographic or photoelectric while later observations are all CCD-based (in blue). The bar in the *top right* area of the V11 *panel* indicates the range of dates shown in Fig. 2. The magnitude scale tick marks show 0.05 mag intervals.

the *I*-band only data after 1990 are available. The derived amplitudes are given in columns 7–9 of Table 7 where the values have uncertainties of 0.03 mag in *V* and I_C and 0.05 mag in *B*. The *U*-band observations are uncertain and limited and we did not attempt to derive amplitudes in *U*.

In Fig. 4a we show the derived B, V and I_C amplitudes as a function of M_V. A star's M_V reflects its evolutionary state with a brighter value being a star farther up the red giant (or asymptotic) branch with cooler surface temperature, larger radius, lower mean density, and subtly differing internal structure including depth and strength of convective energy transport. These properties are all tied to pulsation behavior, particularly the mean density that determines the resonant modes of a star and the depth of the partial ionization zones that provide the opacity "valve" that plays a role in driving red giant pulsation (see Catelan and Smith 2015). It is clear from Fig. 4a that as metal-poor stars reach an evolutionary state corresponding to $M_V \approx -2.25$ mag, the strength of pulsation, as measured by photometric amplitude, begins to increase rapidly. As is true of Cepheid and RR Lyr pulsators, we observe the amplitudes to be largest in the shorter-wavelength passbands. These results should help in constraining and refining models of red giant pulsation, including those that incorporate convection (*cf.* Olivier and Wood 2006).

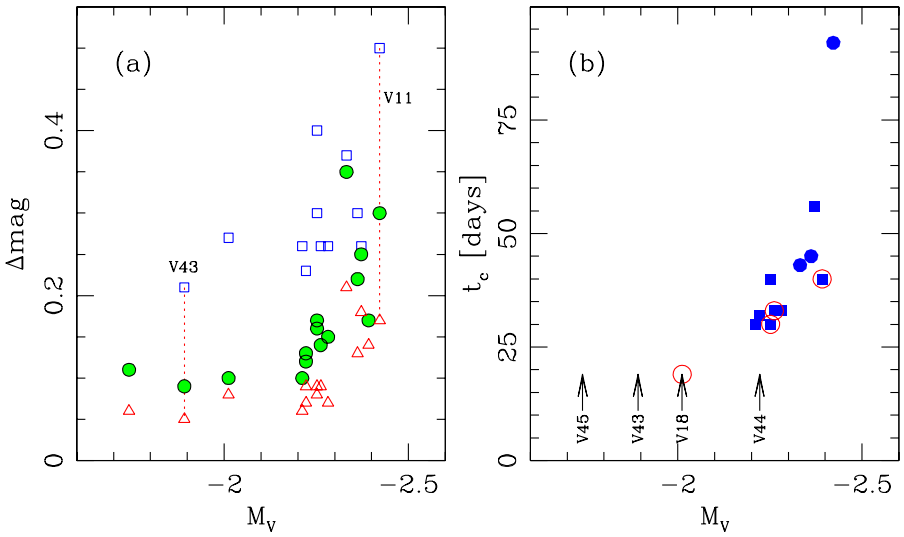

Fig. 4. *Panel a*: Amplitude, or range of variation, of the red variables as a function of absolute magnitude from Table 7. The B, V, and I_C data are represented as open squares, solid circles, and open triangles, respectively. The points in the three passbands for V11, the brightest star, and for V43, the faintest with data in all three passbands, are linked with lines. The decreasing amplitude with both wavelength and absolute magnitude is obvious. *Panel b*: Characteristic cycle time of the M13 red variables as a function of M_V. Stars assigned to type SRb are plotted as dots and those to type SR as squares. Objects for which we found long secondary periods are circled. Arrows mark the absolute magnitudes of the L stars (those for which we could not discern persistent cyclicity).

3.4. Variability Timescales and Variable Classifications

Section 2 of KKP03 gives a history of the study of the M13 variables to 2001, including the red variables and the attempts to determine their periods. Notable work since includes considerable observations, and some analysis, done by the Violat Team. Their papers typically provide, for one or more stars, a seasonal

light curve and its characteristics – mean magnitude, amplitude and periodicities detected. The individual observations are not presented. Because most of this work is not discoverable through the professional literature we have made a conscious effort to summarize their results, particularly in our star-by-star discussion in the Appendix.

Previous papers often have presented periods for one or more of the M13 variables, at times with four significant figures, but those usually disagree and sometimes significantly. For example, suggested periods for V15 include 39.23 d (Osborn and Fuenmayor 1977), 72.0 d (VB15) and 140.3 d (Russev and Russeva 1979c). The inconsistencies likely are due to two factors that complicate any search for periodicities. First, the brightness variations of red giants usually are, at best, only semiregular with significant changes in the light curve shape and duration from one cycle to another and can involve multiple interacting periods. Second, the observations – ours as well as those in the literature – consist of "seasons" of data taken mostly during the Northern summer and typically lasting ≤ 130 d. Such time coverage means each season typically samples only one to three variation cycles while the significant gaps between seasons coupled with light curve changes makes linking behavior from one season to another difficult. We therefore prefer, in place of period, to characterize the variations with an average cycle time, defined as a typical time from one maximum to the next for a given star and recognizing that the duration of any particular cycle may deviate significantly from the average.

An attempt to characterize a semi-regular or irregular variable from only a few variation cycles can lead to mis-representations of the typical cycle time and light-curve regularity. For example, while the CCD data of KKP03 clearly show the light curve behavior for the red variables they observed (see their Fig. 5), their time span of $\sim$90 nights is insufficient to determine periodicities except for V41 which has a well-defined 42.5 d period as discussed below. We proceeded adopting the philosophy that the best characterization of a star's light curve will result from considering together all long and good-coverage observation sets in order to sample and span as many cycles as possible. We believe our large aggregate data, consisting of new CCD observations and much unpublished photographic data combined with a systematic analysis of all published results, including the good coverage observations by the Violat Team, provide the clearest picture to date of these stars' variability, including the general lack of regularity in cycle time, amplitude, and light curve shape.

For each star we first examined the light curves from the new and published work and looked at their differences and the variations in cycle time. We then searched those data sets with good time coverage for periodicities of significant power. The period search employed the Date Compensated Discrete Fourier Transform method, as implemented in the program VSTAR (Benn 2012)[7]. For the majority of the stars we were able to identify a typical cycle time. Several stars also

[7] Available at *https://www.aavso.org/vstar-overview*.

gave evidence for a long secondary period (LSP) of the type described by Percy *et al*. (2004) and Wood *et al*. (2004) underlying the shorter timescale variations.

The periodicity results were used to adopt the star's variability classification. Using the definitions in the *General Catalogue of Variable Stars*,[8] we classified the stars as SRb, SR or L-type. SRb indicates those stars showing both fairly persistent periods and evidence of interacting short (not LSP) periods; SR-type are those stars with less persistent periods and inconclusive evidence of interacting periods; L-type are those cases with little or very weak evidence of periodicity. It is likely that many of the stars we list as types SR and L will be eventually reclassified as SRb once additional, better time-coverage observations become available, as has been demonstrated by the OGLE team's work on the LMC (Soszyński *et al*. 2009).

T a b l e 8

Absolute magnitude, variablity type, "periods" and mean K_S and W_I magnitudes

Star	M_V [mag]	Type	t_c [d]	LSP [d]	K_S [mag]	W_I [mag]
V11	−2.42	SRb	92		8.465	12.18
V42	−2.29	SR	40	320	8.449	12.39
V39	−2.37	SR	56		8.418	12.28
V24	−2.36	SRb	45		8.335	12.11
V17	−2.33	SRb	43		8.452	12.41
V33	−2.28	SR	33		8.568	12.37
V40	−2.26	SR	33	170:	8.732	12.67
V20	−2.25	SR:	40:		8.527	12.35
V19	−2.25	SR	30:	168:	8.618	12.50
V38	−2.22	SR	32:		8.736	12.58
V44	−2.22	L			8.417	12.79
V15	−2.21	SR	30:		8.763	12.65
V18	−2.01	L		200	9.242	13.10
V43	−1.89	L			9.460	13.35
V45	−1.74	L			9.695	13.88
V41	−1.19	ELL/E	42.5		10.443	14.40
V32	−0.21	SR	33:		12.213	16.22

Notes: K_S for V44 probably affected by its close companion. The V41 period search yielded 42.5 d but the true period may be twice that as discussed below.

The details of our analyses for the variables are provided in the Appendix, except for the unusual variable V41 which is discussed below. Our derived variable types, average cycle times and LSP's are given in Table 8 which lists the stars in order of average absolute magnitude. These cycle times, being based on data with extensive time coverage and taking into account previous period-search findings,

[8] see *http://www.sai.msu.su/gcvs/gcvs/vartype.htm*

will be adopted as the best "periods" of the stars for the discussions that follow. We note that SRb stars often show alternating high and low levels of maximum and/or minimum and a cycle time double that listed may at times better describe the light curve. Table 8 also gives single-epoch K_S magnitudes from 2MASS (Skrutskie *et al*. 2006) and the almost reddening-free I_C-band Wesenheit index W_I (as defined in Soszyński *et al*. 2007) which are utilized below.

Long-Term Secular Changes

We briefly note that in those cases where we had observations covering at least a decade we examined them for long-term changes in average brightness. None was detected, including for V11 whose combined B and m_{pg} observations span over fifty years (1962 to 2014).

The Interesting Case of V41

This star is too faint and blue to be a traditional red variable (see Fig. 1). KKP03 found the variations of V41 to be regular with a period of 42.5 d. This was confirmed by the Violat Team[9]. A period search on our combined V data in the range 0.3–100 d yielded a clear period of 42.50 d. No other significant periodicities were found. The phased V light curve using our derived period is shown in the left part of Fig. 5 where nightly averages have been used for the more uncertain BGSU, MSU and Macalester data.

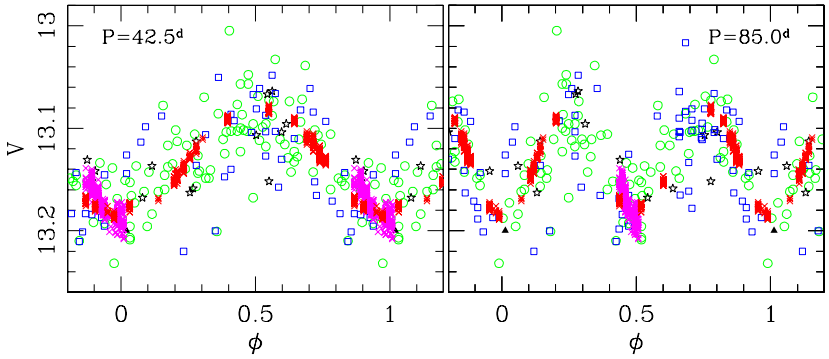

Fig. 5. Phased V-band light curve for V41 with periods of 42.5 d (*left*) and 85.0 d (*right*). The symbols indicate data from: Białków 2001 – crosses (red), Białków 2014 – crosses (magenta), BGSU – open circles (green), Macalester – open stars (black), MSU – open squares (blue), Welty – solid triangle (black).

Hut *et al*. (1992) listed V41 = L782 as a likely binary on the basis of its radial velocity variations. The available photometric observations can be fit equally well with a period of 85.0 d, double 42.5 d (see VA07b), opening the possibility that V41 is an ellipsoidal binary like those found in the Large Magellanic Cloud (LMC) by Soszyński *et al*. (2004b). Our I_C-band amplitude of 0.12 mag is in good agreement with the range of amplitudes shown in Fig. 1 of Soszyński *et al*. (2004b)

[9] *http://casanchi.com/ast/v41.pdf*, hereafter VA07b

but shows no evidence of a direct eclipse which is seen in about 8 per cent of their sample (see their Fig. 2). Our light curve for V41 using the presumed orbital period of 85.0 d (see right side of our Fig. 5) has a similar sinusoidal behavior as the LMC ellipsoidal variables. The alternating minima of the LMC stars tend to differ by a few hundredths of a magnitude. Those of V41 appear to be equal, though the observational scatter in Fig. 5 makes this difficult to ascertain. A contemporaneous photometric and radial velocity survey, like that of Nicholls, Wood and Cioni (2010), would clarify whether the brightness variations of V41 are pulsational or orbital.

3.5. The Period–Luminosity Relation

Fig. 4b plots cycle time as a function of M_V, with our SRb variables shown as circles and SR types as squares. Red-circled symbols indicate stars for which we found long secondary periods. One sees a tendency for more the luminous, and hence more evolved, stars to have more regular pulsation (SRb *vs*. L classification) while the presence of a LSP seems to occur without preference to luminosity. It is the least luminous stars for which we could not find persistent periodicity. A correlation between cycle time and absolute magnitude is seen for the rest. Such PL relations for red variables are now well known, particularly from the extensive data produced by the microlensing campaigns such as OGLE (Soszyński *et al*. 2007, 2009). We next compare our PL results with those from other stellar systems.

Comparison of M13 and Large Magellanic Cloud Red Variable PL Diagrams

A number of authors have presented the locations in the PL plane of red variables in the Large Magellanic Cloud (LMC) utilizing the extensive data from the various microlensing campaigns. Fig. 6 shows the results for the LMC from Fig. 1 of Kiss and Lah (2006) which was based largely on the work of Wood (2000), Ita *et al*. (2004a) and Kiss and Bedding (2003, 2004a, 2004b) and which used K_S magnitudes as the luminosity indicator. The diagram clearly shows several linear sequences which are labeled as per Ita *et al*. (2004b) with the mean lines from their Table 3. Sequence C are stars pulsating in the fundamental (F0) mode while sequences C′, B− and A− are thought to represent first overtone (F1), second overtone (F2) and third overtone (F3) pulsations, respectively. The A and B sequences have distinct breaks at $K_S = 12.05$ mag which correspond to the tip of the red giant branch. The two sequence portions are generally denoted A− and B− for the lower luminosity part and A+ and B+ (not labeled here) for the more luminous sections.

Single epoch near-infrared K_S magnitudes for the M13 red variables are available from 2MASS (Skrutskie *et al*. 2006, see Table 8), and these with our adopted cycle times can be used to prepare a similar diagram for M13. We adopted true distance moduli $(V - M_V)_0$ of 14.27 mag for M13 (Buckley and Longmore 1992, Harris 2010) and 18.49 mag for the LMC (Crandall and Ratra 2015, de Grijs, Wicker and Bono 2014). Adjusting the M13 K_S magnitudes for the different distance of the

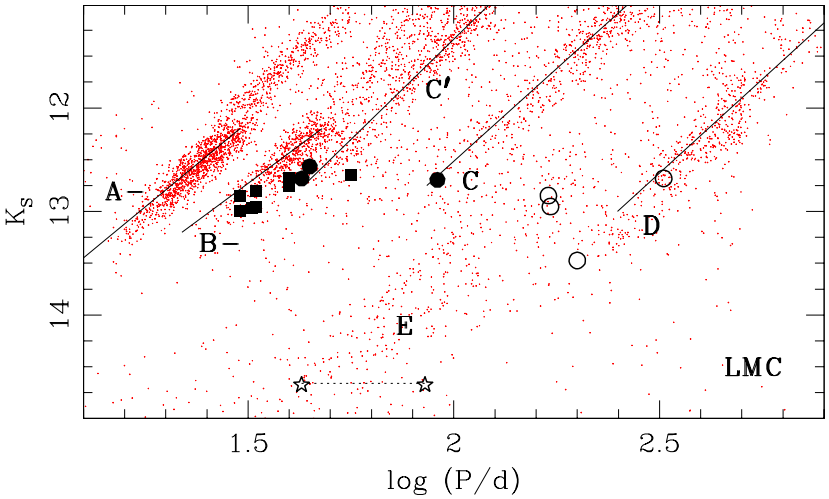

Fig. 6. Period–luminosity diagram for red variables in M13 compared to that for red variables in the Large Magellanic Cloud. The small dots mark the apparent K_S magnitudes of the LMC variables from Ita *et al*. (2004b) with lines showing the centers of the various sequences. The larger points mark red variables in M13, shifted to the respective distance moduli of the Cloud. Stars we classified SRb are filled circles and those called L are filled squares. Variables found to have long secondary periods are also plotted using that period (open circles). V41 is plotted with both of its two possible periods (the connected star symbols).

LMC, we can compare the M13 red variables to the LMC results and these stars' positions have been added to Fig. 6. We again plot stars we classified as SRb as filled circles and those called SR as filled squares.

Most of the M13 stars fall close to the sequences for F1 and F2 pulsators. The notable exceptions are V11, where its relatively-long 92 d period indicates pulsation in the fundamental mode, and the fainter regular variable V41. V41 is plotted using both possible periods (open stars) and both cases lie in the E region occupied mostly by ellipsoidal binaries. The four M13 stars for which we tentatively found an LSP are plotted a second time using the the periods in Table 8 (open circles). The two with most certain LSP periods lie along the D sequence. The two others fall where the D and E regions merge but, as discussed in the Appendix, in each case we could not rule a longer possible LSP that would place them clearly in the D region.

M13 Red Variables Compared to Red Variables in Other Globular Clusters

A more extensive plot of the LMC PL relations is shown in Fig. 7 using the data from the OGLE-III catalog of long-period variables (LPVs) compiled by Soszyński *et al*. (2007) with the periods of ellipsoidal binary systems from Pawlak *et al*. (2014). Here luminosity is represented by the I_C-band Wesenheit index W_I. Each star is represented by one point, using the primary period for stars with multiple periodicities.

The sequences seen in Fig. 6 are again visible (now using the labeling of Wood *et al*. 1999 and Soszyński *et al*. 2007), but in the $W_I - \log P$ plane each of the sequences C and C′ splits into two subsequences, one composed of O-

rich stars (green dots in Fig. 6), and the other C-rich ones (red dots). Following Soszyński *et al*. (2007), we designate these subsequences with subscripts "O" and "C", respectively. Mira-type stars are found along sequences C_O and C_C, while bright semiregular variables (SRV) form sequences C'_O and C'_C. The OGLE small-amplitude red giants (OSARGs, Soszyński *et al*. 2004a) are located in sequences A' and A. Sequence B seems to contain both OSARGs and SRVs. Sequences D and E are composed of stars exhibiting LSP's and ellipsoidal systems, respectively. The upper – brighter – part of the diagram is occupied by asymptotic giant branch (AGB) stars while the fainter part is a mixture of AGB and red giant branch (RGB) stars.

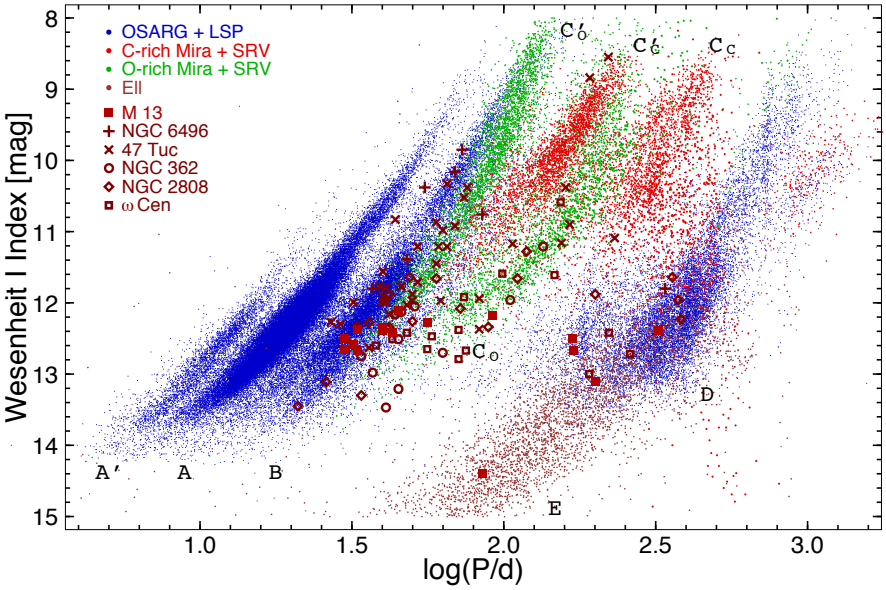

Fig. 7. PL diagram of variable red giants in the LMC, with luminosity expressed using the I_C-band Wesenheit index, from the combined OGLE-II and OGLE-III photometry. OSARGs and variables with LSP's are shown as blue dots. Miras and SRVs are marked with either green dots (O-rich stars) or red dots (C-rich stars) and ellipsoidal systems are indicated with light brown dots. The most prominent sequences are labeled after Wood *et al*. (1999) and Soszyński *et al*. (2007). Superposed on the LMC diagram are the locations of the red variables in six galactic globular clusters.

Superposed on the LMC diagram are the locations of the red variables in six globular clusters (GC) adjusted to the LMC distance. The clusters are M13 (studied here and using the longer period option for V41), 47 Tuc (Lebzelter and Wood 2005), NGC 6496 (Abbas *et al*. 2015), NGC 362 and NGC 2808 (Lebzelter and Wood 2011) and ω Cen (Lebzelter and Wood 2016). These clusters cover a rather wide range of metallicity, from $[Fe/H] = -0.46$ dex for NGC 6496 to -1.53 dex for M13 (Harris 2010), and have been well-surveyed for variables. The distribution of the GC red variables seems to form three distinct sequences that align along four of the LMC sequences. Most stars follow the fainter part of sequence B – the region that is a mix of LMC OSARG and SRV types – up to where the brighter

part of sequence B merges with sequence C'_O which is composed of O-rich SRVs. The longer-period GC variables nicely follow sequence C_O, composed of O-rich Mira stars. Then there is a sizable population of LSP stars which fall on the broad sequence D. We note, however, that the periods for such stars identified in 47 Tuc and NGC 362 (Lebzelter and Wood 2005, 2011) were not published and thus this globular cluster population is underrepresented in the diagram.

The GC red variables align with O-rich (green-colored) sequences as expected. The exceptions are three 47 Tuc variables found by C-rich regions. While stars with enhanced carbon are known in globular clusters (*e.g.*, Harding 1962, Osborn 1971, Wing and Stock 1973, Feast, Menzies and Whitelock 2013), we do not believe that to be the case here. The two very bright stars (47 Tuc V1 and V3) are to the left of – not on – the uppermost portion of the C'_C sequence, a region where O-rich Miras are also common. The fainter star (47 Tuc V20) that lies centrally on the C_C sequence has a very uncertain period (Lebzelter and Wood 2005) and its horizontal position in the diagram is unreliable.

3.6. Metal Dependence of Globular Cluster Red Variables

Fig. 7 shows a tendency for the red variables in the more metal-rich clusters to be brighter. This is seen more clearly in Fig. 8 where we plot red variable luminosity as a function of metal abundance. The two panels use K_S, and W_I for luminosity, the different indicators of Fig. 6 and Fig. 7, with both scaled to the distance of the LMC. The scale on the right-hand side of each panel shows the absolute magnitude of the respective index, computed by subtracting the LMC's distance modulus. The mean cluster [Fe/H] (Harris 2010) has been used for all stars in a given cluster other than for those in ω Cen, which has a large range in metallicity. The ω Cen variables are plotted as smaller symbols at each star's individual [Fe/H], preferring the values listed in column 13 of Table 1 of Lebzelter and Wood (2016). Circles indicate C-sequence (fundamental mode, Mira type) stars, while crosses are the shorter-period overtone pulsators (mainly B− or C′ sequences), but include the "no period" irregular stars as well.

The blue dashed line in the upper panel represents the relation between metal abundance and brightness of the tip of the red giant branch (TRGB) for globular clusters as found by Valenti, Ferraro and Origlia (2004, Eq. 9). Stars above this line are interpreted to be asymptotic branch stars. All (except two very metal-poor ω Cen stars with less certain [Fe/H]) are fundamental mode pulsators. The dotted lines in the two panels are our TRGB relations. For each of the five single-metallicity clusters, we selected the brightest overtone pulsator (cross symbols in Fig. 8) to define the TRGB, and performed a least-squares fit to the cluster metallicities, obtaining:

$$M_K(\mathrm{TRGB}) = (-6.96 \pm 0.09) - (0.65 \pm 0.08)\ [\mathrm{Fe/H}] \quad (2)$$

$$M_W(\mathrm{TRGB}) = (-9.71 \pm 0.34) - (2.36 \pm 0.31)\ [\mathrm{Fe/H}]. \quad (3)$$

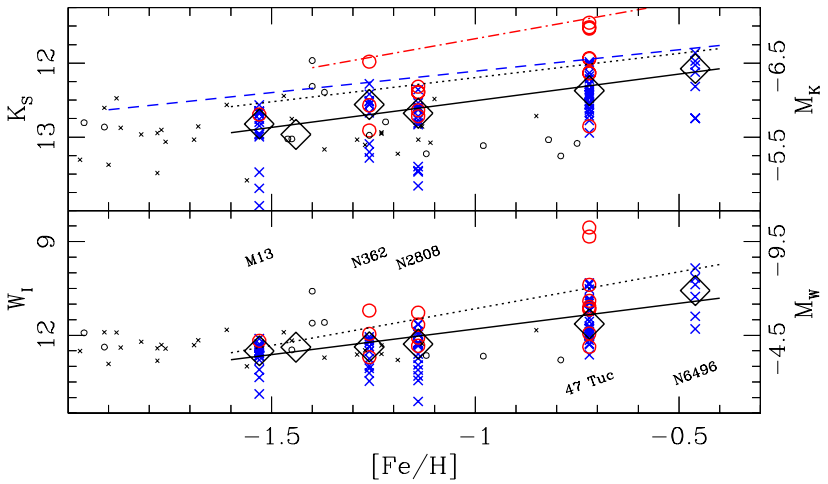

Fig. 8. Relationship between metallicity and absolute magnitude for red variables in Galactic globular clusters. Fundamental pulsators are shown as circles and overtone pulsators as crosses. The clusters are labeled in the *lower panel*, except for ω Cen whose members have a large range in metallicity and are plotted using small symbols. The diamonds indicate the median values for the clusters with the solid lines their least-squares fits. The dotted lines show our fitted relations between cluster metallicity and luminosity of the tip-of-the RGB, while the blue dashed line in the *upper panel* shows that relation as derived by Valenti *et al*. (2004). The red dash-dot line is the metallicity relation for GC Miras.

The *rms* scatter of the fits are 0.05 mag and 0.24 mag for K_S and W_I, respectively. There is close agreement between our K_S result in Eq.(2) and that of Valenti *et al*. (2004) which was based on significantly more clusters.

A second approach to characterizing the luminosity dependence on metallicity for bright red giants is, given the confusion caused by asymptotic branch stars, to use all red variables to create a luminosity measure rather than attempting to identify the "single star" tip of the red giant branch. The brightest red stars in a cluster are all variables (see, for example, Fig. 1), and statistically most will be red giant branch stars. Thus, the red variable locus may better characterize a cluster's uppermost RGB than the more uncertain RGB tip. The diamonds in Fig. 8 indicate the median absolute magnitude and metallicity of the known red variables for the six clusters from Fig. 7 (the unlabeled diamond is for ω Cen). The solid lines show the two least-squares fits:

$$M_K(\text{median}) = (-6.72 \pm 0.13) - (0.72 \pm 0.12)\ [\text{Fe/H}] \quad (4)$$

$$M_W(\text{median}) = (-8.33 \pm 0.36) - (1.64 \pm 0.31)\ [\text{Fe/H}] \quad (5)$$

with the *rms* scatter being 0.09 mag and 0.21 mag for K_S and W_I respectively.

For both the TRGB and the red-variable-median approaches, linear fits do a fair job of describing the dependence of K_S and W_I on metallicity for the five single-metallicity clusters (there is the suggestion that a quadratic function might better fit the Wesenheit index medians). Nevertheless, several factors affect the reliability of these luminosity indicators. First, the quality of the survey for cluster

variable stars determines the detection percentage. Given the correlation between luminosity and amplitude (see Fig. 4a), the fainter variables typically will be the most under-represented, which in turn could compromise the median-brightness determination. Fortunately, all the GC surveys used in Fig. 8 claim similar variability detection limits of a V amplitude of 0.05 mag to 0.10 mag, so any effect on the median points should be small. Second, the more massive a cluster is the more likely it will have a well-populated luminosity function and therefore more red variables and a better determined luminosity indicator. In Fig. 8, one can compare the data for 47 Tuc with those for NGC 6496, these being examples of large- and small-mass clusters based on their integrated absolute magnitudes, $M_V^{\rm tot}$ (Harris 2010). Finally, the TRGB and variable-median luminosities may be affected by cluster-to-cluster variations in factors other than metallicity, such as age (main sequence turn-off mass), mass loss rate on the giant branch, or helium abundance as discussed in Lebzelter and Wood (2005, 2011, 2016).

The fits in Fig. 8 do a poorer job of describing the red variables in ω Cen. While the larger errors of the abundances of these individual stars add horizontal uncertainty to the plotted points, the absolute magnitudes of these stars seem to get fainter systematically with increasing metallicity. This trend can be explained, qualitatively at least, as follows. Lebzelter and Wood (2016) showed that the metal-rich variables of ω Cen ([Fe/H] > -1.4 dex) are best described with an enhanced helium abundance, and their helium-enhanced models place the TRGB significantly fainter than in standard models.

Finally, we note that Whitelock, Feast and van Leeuwen (2008) derived a relation between M_K and $\log P$ for globular cluster Miras, defined as the large-amplitude and long-period AGB variables found in the more metal-rich clusters. Earlier, Feast and Whitelock (2000) found a correlation between [Fe/H] and $\log P$ for such stars. Combining the two relationships one derives

$$M_K = -7.82 - 0.98\ [\mathrm{Fe/H}] \qquad (6)$$

for the absolute magnitude dependence on metallicity for GC Miras. This relation is shown by the red dash-dot line in the top panel of Fig. 8. It fits well the six AGB stars (the fundamental-mode pulsators above the TRGB line) in our data (V1, V2 and V3 in 47 Tuc, V16 in NGC 362, V6 and V42, the brightest ω Cen stars at $[\mathrm{Fe/H}] = -1.4$ dex), all of which have $P \geq 135$ d and $\Delta V \geq 2.4$ mag (C13, Lebzelter and Wood 2016). This result and Eqs.(2–5) from clusters with a wider range of metallicity clearly indicate that the luminosity of CG red variables is significantly affected by metallicity, an effect that needs to be taken into account when modeling the variability of low-mass red giants, or in using them as distance indicators. Indeed, the metallicity dependence nicely accounts for M13 sequences falling somewhat below those of the LMC (see Fig. 6). The lower metallicity of the M13 variables makes them less luminous than the LMC variables of the same period.

4. Summary and Conclusions

New CCD and unpublished photoelectric and photographic observations combined with a systematic analysis of all published data provide a clearer picture of the variability of the red variables in the globular cluster M13. We have determined mean magnitudes and colors on the $UBVI_C$ system for the seventeen stars so classified. Fifteen are traditional red variables that lie at the top of the red giant branch in the color–magnitude diagram, two stars – V32 and V41 – are not top-of-the-RGB variables. Data on V32 are sparse but it appears to be a low-amplitude variable with a period around 30 d. V41 has a well-defined period of 42.5 d. The light curve shape indicates it is an ellipsoidal, or possibly eclipsing, variable with a true period of 85.0 d. All M13 red giants with $(V - I_C)_0$ greater than 1.38 mag, equivalent to stars brighter (more evolved) than $M_V = -2.25$ mag, have been confirmed to vary.

For the traditional red variables, all have variations that are at best semi-regular and show changes in the amplitude, shape and cycle duration of the light curve from cycle to cycle. Alternating high and low levels of maximum and/or minimum often occur. The full amplitude of the variation increases with absolute magnitude and bluer color, reaching 0.50 mag in the *B*-band for the most luminous star, V11. Searches on the data sets reveal some periodicities, but these often are not persistent. We instead characterize the variations with an average cycle time, defined as a typical time from one maximum to the next for a given star and recognizing that the duration of any particular cycle may deviate significantly from the average.

Our derived cycle times range from 30 d to 92 d. They correlate with absolute magnitude, being longer and having larger ranges of brightness for those variables that are the most luminous and more evolved. No long-term secular effects were detected. We believe our derived cycle times, which are based on analyses of data with extensive time coverage as well as taking into account previous findings, should supersede and be used in place of all previous estimates of periods.

Our CCD data suggest that persistent multiple periods are acting in the variations of V11, V17 and probably V24 and we therefore recommend characterizing these variables as semi-regular SRb type. Lasting periodic behavior was found for V33, V40, V39 and V42 and with less certainty for V15, V20, V19, V32, and V38. We therefore classify these as SR type. No persistent periodicities were found for V18, V43, V44 and V45 and these have been assigned L-type. Improving on the periods and the variable type assignments presented here will need several years of year-round observational coverage with at least 2–3 d cadence in order to provide a time-series data capable of following the variations sufficiently long to distinguish multiperiodic behavior from truly aperiodic changes and to reliably characterize the long secondary periods in these stars. One or more robotically-operated, 0.5-m class telescopes at good, northern-hemisphere dark sites should be capable of providing the low-noise data required for such a study.

The locations of the M13 red variables in the PL plane are mostly on the B− and C′ sequences found in the Large Magellanic Clouds from its extensive mi-

crolensing data. This indicates overtone pulsation. Combining the M13 data with those from other surveys of red variables in galactic globular clusters shows the cluster red variables have similar PL sequences to those seen in the LMC. These observations also show a correlation between cluster metal abundance and luminosity for both RGB and AGB variables as shown in Fig. 8 and quantified in Eqs.(2–6). Studies of red variables in additional clusters, particularly of lower metallicity than those represented here, would refine the RGB relation. In this regard, we mention that the photographic study of the metal-poor cluster NGC 2419 ($[\mathrm{Fe/H}] = -2.15$) by Pinto and Rosino (1977) identified four red variables. CCD-based photometry for their confirmation and light curves along with a search for other such variables in the cluster would be of value.

Acknowledgements. We thank the anonymous reviewer for raising several points, our consideration of which led to improvements in the paper. GK acknowledges the support from NCN grant no. 2011/03/B/ST9/02667. HS thanks the U.S. National Science Foundation for partial support of this work under grants AST0440061, AST0607249, and AST0707756. We also thank R. Russev and D. Welty for providing their unpublished observations. This research has utilized the online resources of the American Association of Variable Star Observers, the SAO/NASA Astrophysics Data System, the SIMBAD database, operated at CDS, Strasbourg, France, and data from the Two Micron All Sky Survey, which was a joint project of the University of Massachusetts and the Infrared Processing and Analysis Center/California Institute of Technology, funded by the National Aeronautics and Space Administration and the National Science Foundation.

REFERENCES

Abbas, M.A., Layden, A., Guldenschuh, K.A., Reichart, D.E., Ivarsen, K.M., Haislip, J.B., Nysewander, M.C., LaCluyze, A.P., and Welch, D.L. 2015, *AJ*, **149**, 40.
Alard, C., and Lupton, R.H. 1998, *ApJ*, **503**, 325.
Arp, H.C., and Johnson, H.L. 1955, *ApJ*, **122**, 171.
Bailey, S.I. 1902, *Harvard Annals*, **38**, 1.
Benn, D. 2012, *JAAVSO*, **40**, 852.
Bessell, M.S. 1990, *PASP*, **102**, 1181.
Bergbusch, P.A., and Stetson, P.B. 2009, *AJ*, **138**, 1455.
Buckley, D.R.V., and Longmore, A.J. 1992, *MNRAS*, **257**, 731.
Catelan, M., and Smith, H.A. 2015, in: "Pulsating Stars", Wiley-VCH, Weinheim (Germany), p. 215.
Cathey, L.R. 1974, *AJ*, **79**, 1370.
Cohen, R.L., Guhathakurta, P., Yanni, B., Schneider, D.P., and Bahcall, J.N. 1997, *AJ*, **113**, 669, (CGY).
Cook, K.H., *et al*. 1995, *ASP Conf. Series*, **83**, 221.
Crandall, S., and Ratra, B. 2015, *ApJ*, **815**, 87.
Cudworth, K. 1979, *AJ*, **84**, 1005.
Cudworth K., and Monet, D.G. 1979, *AJ*, **84**, 774.
de Grijs, R., Wicker, J.E., and Bono, G. 2014, *AJ*, **147**, 122.
Demers, S. 1971, *AJ*, **76**, 445.

Feast, M., and Whitelock, P. 2000, in: "The Evolution of the Milky Way: stars versus clusters", Eds. Matteucci, F., and Giovannelli, F. (Kluwer Academic Publishers) p. 229.
Feast, M.W., Menzies, J.W., and Whitelock, P.A. 2013, *MNRAS*, **428**, L36.
Frogel, J.A., and Elias, J.H. 1988, *ApJ*, **324**, 823.
Guarnieri, M.D., Bragaglia, A., and Fusi Pecci F. 1993, *A&AS*, **102**, 397, (GBF).
Harding, G.A. 1962, *The Observatory*, **82**, 205.
Harris W.E. 2010, arXiv:1012.3224.
Hut, P., McMillan, S., Goodman, J., *et al*. 1992, *PASP*, **104**, 981.
Ita, Y., Tanabé, T., Matsunaga, N., Nakada, Y., and IRSF/SIRIUS Team 2004a, *ASP Conf. Series*, **310**, 50.
Ita, Y., *et al*. 2004b, *MNRAS*, **347**, 720.
Kadla, Z.I. 1966, *Izvestiia Glavnoi astronomicheskoi observatorii v Pulkove*, **24**, 93.
Kim, D.-W., Protopapas, P., Bailer-Jones, C.A.L., Byun, Y.-I., Chang, S.-W., Marquette, J.-B., Shin, M.-S. 2014, *A&A*, **566**, A43.
Kiss, L.L., and Bedding, T.R. 2003, *MNRAS*, **343**, L79.
Kiss, L.L., and Bedding, T.R. 2004a, *ASP Conf. Series*, **310**, 55.
Kiss, L.L., and Bedding, T.R. 2004b, *MNRAS*, **347**, L83.
Kiss, L.L., and Lah, P. 2006, *Memorie della Societa Astronomica Italiana*, **77**, 303.
Kopacki, G., Kołaczkowski, Z., and Pigulski, A. 2003, *A&A*, **398**, 541, (KKP03).
Kopacki, G., Drobek, D., Kołaczkowski, Z., and Połubek, G. 2008, *Acta Astron.*, **58**, 373.
Landolt, A.U. 1983, *AJ*, **88**, 439.
Landolt, A.U. 1992, *AJ*, **104**, 340.
Lebzelter, T., and Wood, P.R. 2005, *A&A*, **441**, 1117.
Lebzelter, T., and Wood, P.R. 2011, *A&A*, **529**, A137.
Lebzelter, T., and Wood, P.R. 2016, *A&A*, **585**, A111.
Ludendorff, H. 1905, *Publikationen des Astrophysikalischen Observatoriums zu Potsdam*, **15**, F1.
Menzies, J.W., Marang, F., Laing, J.D., Coulson, M., and Engelbrecht, C.A. 1991, *MNRAS*, **248**, 642.
Nicholls, C.P., Wood, P.R., and Cioni, M.-R.L., and Soszyński, I. 2009, *MNRAS*, **399**, 2063.
Nicholls, C.P., Wood, P.R., and Cioni, M.-R.L. 2010, *MNRAS*, **405**, 1770.
Olivier, E.A., and Wood, P.R. 2006, *Memorie della Societ Astronomica Italiana*, **77**, 515.
Osborn, W. 2000, *AJ*, **119**, 2902.
Osborn, W.H. 1971, *The Observatory*, **91**, 223.
Osborn, W., and Fuenmayor, F. 1997, *AJ*, **82**, 395.
Pawlak, M., *et al*. 2014, *Acta Astron.*, **64**, 293.
Percy, J.R., Bakos, A.G., Besla, G., Hou, D., Velocci, V., and Henry, G.W. 2004, *ASP Conf. Series*, **310**, 348.
Pike, C.D., and Meston, C.J. 1977, *MNRAS*, **180**, 613.
Pinto, G., and Rosino, L. 1977, *A&AS*, **28**, 427.
Rey, S.-Ch., Yoon, S.-J., Lee, Y.-W., Chaboyer, B., and Sarajedini, A. 2001, *AJ*, **122**, 3219.
Russev, R.M. 1973, *Peremennye Zvezdy*, **19**, 181.
Russev, R.M., and Russeva, T. 1979a, *IBVS*, 1534.
Russev, R.M., and Russeva, T. 1979b, *IBVS*, 1624.
Russev, R.M., and Russeva, T.S. 1979c, *Peremennye Zvezdy*, **21**, 169.
Russeva, T.S., and Russev, R. 1980, *IBVS*, 1769.
Russeva, T.S., Illiev, L., and Russev, R. 1982, *IBVS*, 2223.
Sandquist, E.L., Gordon, M., Levine, D., and Bolte, M. 2010, *AJ*, **139**, 2374.
Schild, R.E. 1983, *PASP*, **95**, 1021.
Schild, R.E. 1985, *PASP*, **97**, 824.
Schultheis, M., Glass, I.S., and Cioni, M.R. 2004, *A&A*, **427**, 945.
Skrutskie, M.F., *et al*. 2006, *AJ*, **131**, 1163.
Soszyński, I., *et al*. 2004a, *Acta Astron.*, **54**, 129.
Soszyński, I., *et al*. 2004b, *Acta Astron.*, **54**, 347.

Soszyński, I., *et al*. 2007, *Acta Astron*., **57**, 201.
Soszyński, I., *et al*. 2009, *Acta Astron*., **59**, 239.
Soszyński, I., Wood, P.R., and Udalski, A. 2013, *ApJ*, **779**, 167.
Stetson, P.B. 1987, *PASP*, **99**, 191.
Stetson, P.B. 1994, in: "Astronomy with the CFHT Adaptive Optics Bonnette", Proceedings of the Workshop held in Quebec City, P.Q., Canada, May 1994, Ed. Arsenault, R., p. 72.
Stetson, P.B. 2000, *PASP*, **112**, 925.
Takayama, M., Saio, H., and Ita, Y. 2013, *MNRAS*, **431**, 3189.
Valenti, E., Ferraro, F.R., and Origlia, L. 2004, *MNRAS*, **354**, 815.
Violat Bordonau, F.A., Arranz Heras, T., and Díez Gago, A. 2006, *Open European Journal on Variable Stars*, **19**, 1.
Wehlau, A., and Bohlender, D. 1982, *AJ*, **87**, 780.
Welty, D.E. 1985, *AJ*, **90**, 2555.
Whitelock, P.A, Feast, M.W., and van Leeuwen, F. 2008, *MNRAS*, **386**, 313.
Wing, R.F., and Stock, J. 1973, *ApJ*, **186**, 979.
Wood, P.R., *et al*. 1999, *IAU Symp*, **191**, 151.
Wood, P.R. 2000, *Publications of the Astronomical Society of Australia*, **17**, 18.
Wood, P.R., Olivier, E.A., and Kawaler, S.D. 2004, *ApJ*, **604**, 800.